International Journal of
Molecular Sciences

MDPI

Article

The Mitochondrial Ca^{2+} Overload via Voltage-Gated Ca^{2+} Entry Contributes to an Anti-Melanoma Effect of Diallyl Trisulfide

Chinatsu Nakagawa [1,2], Manami Suzuki-Karasaki [2], Miki Suzuki-Karasaki [2], Toyoko Ochiai [1,2] and Yoshihiro Suzuki-Karasaki [2,*]

1 Department of Dermatology, Nihon University Hospital, Tokyo 101-830, Japan; chinatsu.y0503@gmail.com (C.N.); toochiai@j.com.home.net.jp (T.O.)
2 Plasma ChemiBio Laboratory, Nasushiobara, Tochigi 329-2813, Japan; ksmanami181@gmail.com (M.S.-K.); ksmiki181@gmail.com (M.S.-K.)
* Correspondence: yoshisk181@pcbl.or.jp; Tel.: +81-0287-35-3276

Received: 20 December 2019; Accepted: 8 January 2020; Published: 13 January 2020

Abstract: *Allium* vegetables such as garlic (*Allium sativum* L.) are rich in organosulfur compounds that prevent human chronic diseases, including cancer. Of these, diallyl trisulfide (DATS) exhibits anticancer effects against a variety of tumors, including malignant melanoma. Although previous studies have shown that DATS increases intracellular calcium (Ca^{2+}) in different cancer cell types, the role of Ca^{2+} in the anticancer effect is obscure. In the present study, we investigated the Ca^{2+} pathways involved in the anti-melanoma effect. We used melittin, the bee venom that can activate a store-operated Ca^{2+} entry (SOCE) and apoptosis, as a reference. DATS increased apoptosis in human melanoma cell lines in a Ca^{2+}-dependent manner. It also induced mitochondrial Ca^{2+} ($Ca^{2+}{}_{mit}$) overload through intracellular and extracellular Ca^{2+} fluxes independently of SOCE. Strikingly, acidification augmented $Ca^{2+}{}_{mit}$ overload, and Ca^{2+} channel blockers reduced the effect more significantly under acidic pH conditions. On the contrary, acidification mitigated SOCE and $Ca^{2+}{}_{mit}$ overload caused by melittin. Finally, Ca^{2+} channel blockers entirely inhibited the anti-melanoma effect of DATS. Our findings suggest that DATS explicitly evokes $Ca^{2+}{}_{mit}$ overload via a non-SOCE, thereby displaying the anti-melanoma effect.

Keywords: diallyl trisulfide; melittin; melanoma; apoptosis; mitochondrial Ca^{2+}; store-operated Ca^{2+} channel; acidification; Ca^{2+} channel blocker; voltage-gated Ca^{2+} channel

1. Introduction

Allium vegetables such as garlic (*Allium sativum* L.) are rich in allyl sulfides that have been shown to prevent human chronic diseases, including cancer [1]. L-alliin (S-allyl-L-cysteine sulfoxide) is the major allyl sulfide component in garlic, which is converted into 2-propensulfenic acid by the endogenous enzyme alliinase, thereby producing the unstable thiosulfinate compound allicin (*S*-allyl-2-prop-2-ene-thiosulfinate). Allicin readily breaks down to form organosulfur compounds (OSCs), including allyl sulfides such as diallyl trisulfide (DATS), diallyl disulfide (DADS), and diallyl sulfide (DAS), as well as ajoene and vinyl dithiins [2]. OSCs can modulate the immune system and attenuate inflammation, and these effects contribute to cancer prevention [3]. DATS, DADS, and DAS are known to prevent the well-characterized chemical-induced skin carcinogenesis [4–6]. Moreover, the OSCs have anticancer activity in a variety of cancer cell types, including skin cancer such as melanoma and basal cell carcinoma [7]. Of these, DATS is the most widely studied. This compound induces apoptosis in a range of cancer cells, including malignant melanoma, osteosarcoma, and leukemia [8–11].

DATS also potentiates apoptosis induced by tumor necrosis factor-related apoptosis-inducing ligand (TRAIL) in human prostate cancer and melanoma cells [12–14]. The induction and amplification of apoptosis are associated with activation of caspases, upregulation of multiple pro-apoptotic molecules, including death receptor (DR)4/DR5, Bax, and Bak as well as downregulation of anti-apoptotic molecules such as Bcl-2 and Bcl-xL [10]. Fully activation of TRAIL-induced apoptosis in melanoma cells requires not only the intrinsic mitochondrial pathway but also the endoplasmic reticulum (ER) stress pathway [14]. The observations are consistent with the clinical findings that TRAIL can activate robust intrinsic death signaling but are ineffective in drug-resistant cancers, including malignant melanoma [15,16]. Strikingly, DADS and DATS exhibit the anticancer and TRAIL-sensitizing effects in a tumor-selective manner [8,14], and they commonly induce the intracellular generation of reactive oxygen species (ROS) [8,9]. These observations support the view that oxidative stress plays a vital role in the cancer cell-selective killing and TRAIL sensitization [17–19].

Ca^{2+} is a highly versatile intracellular second messenger that regulates numerous complicated cellular processes, including cell activation, proliferation, and death. The increase in the cytosolic Ca^{2+} concentration ($[Ca^{2+}]_{cyt}$) results in the activation of Ca^{2+}/calpain, an intracellular Ca^{2+}-dependent cysteine protease, thereby resulting in the processing of the mitochondrial localized pro-apoptotic molecule, apoptosis-inducing factor, and caspase-independent apoptosis. The activation of Ca^{2+}/calpain occurs during the apoptosis of glioblastoma and neuroblastoma induced by DAS, DADS, and DATS [8,9]. Meanwhile, an excess rise in the mitochondrial Ca^{2+} concentration ($[Ca^{2+}]_{mit}$) leads to increased permeability of the mitochondrial membrane, mitochondrial dysfunction, and release of pro-apoptotic molecules such as cytochrome c and Apaf-1, resulting in caspase-dependent apoptosis. Store-operated Ca^{2+} entry (SOCE) is the principal route by which external Ca^{2+} enters in non-excitable cells. Ca^{2+} depletion in the endoplasmic reticulum (ER) triggers SOCE. The depletion induces the translocation of stromal interaction molecules 1 (STIM1) to ER/plasma membrane (PM) junctional regions, where the molecule activates the PM channel ORAI1, leading to Ca^{2+} entry from the extracellular milieu. Recently, Gualdani and colleagues reported that SOCE mediates cisplatin-induced $Ca^{2+}{}_{mit}$ overload, ROS production, and apoptosis [20].

Melittin, a 26-amino acid amphipathic peptide from bee venom, exhibits the anticancer effect against a variety of tumor cells, including melanoma, leukemia, osteosarcoma, lung, and bladder cancer cells. Melittin induces apoptosis in these tumor cells in a caspase-dependent manner [21–23]. Moreover, earlier studies have suggested that melittin induces apoptosis through Ca^{2+} entry [23,24]. Notably, melittin is also known to activate SOCE via the activation of Ca^{2+}-independent phospholipase A_2 ($iPLA_2$) [25,26]. Collectively, by analogy with cisplatin, it is plausible to speculate that melittin exhibits the anticancer effect through Ca^{2+} overload via SOCE. While DATS preferentially acts on tumor cells [8,14], melittin acts non-specifically, as cisplatin does. Therefore, the identification of the Ca^{2+} transport pathways preferentially activated by DATS may help to define the Ca^{2+} pathways targeted in future tumor-selective therapy.

In the present study, we explored the ability of DATS to cause Ca^{2+} dysregulation and its possible role in the anti-melanoma effect using melittin as a reference. We found that DATS explicitly induces massive Ca^{2+} dysregulation and apoptosis through a voltage-gated Ca^{2+} entry (VGCE) pathway that is distinct from SOCE.

2. Results

2.1. DATS Reduces Cell Viability and Increases Apoptosis in a Ca^{2+}- and Caspase-Dependent Manner

We treated human malignant melanoma cell lines A375 and A2058 with varying concentrations of DATS for 72 h and measured cell viability by using the WST-8 assay. Based on our previous study, we determined the range of the concentrations examined [14]. DATS (≥100 μM) decreased the viability of A375 cells in a dose-dependent manner (Figure 1A). DATS also reduced the viability of A2058 in a dose-dependent manner (Figure 1B). However, cellular sensitivity to DATS varied considerably in

different experiments. As a result, the IC_{50} values for A375 and A2058 cells were 159 ± 32 and 228 ± 60 μM, respectively (the mean ± SD, n = 3–6). Flow cytometric analyses using annexin V and PI staining revealed that 72-h-treatment with DATS (100 μM) alone resulted in a massive increase in apoptotic (annexin V-positive) cells. TRAIL markedly augmented the effect while the pan-caspase inhibitor Z-VAD-FMK entirely blocked it (Figure 1C,D). We found that Ca^{2+} was a critical regulator of drug sensitivity. Treatment with the extracellular Ca^{2+} chelator EGTA (≤0.5 mM) or the intracellular Ca^{2+} chelator BAPTA had minimal effect on cell viability. However, these chelators significantly reduced the anticancer effect of DATS in A375 and A2058 cells (Figure 1E,F).

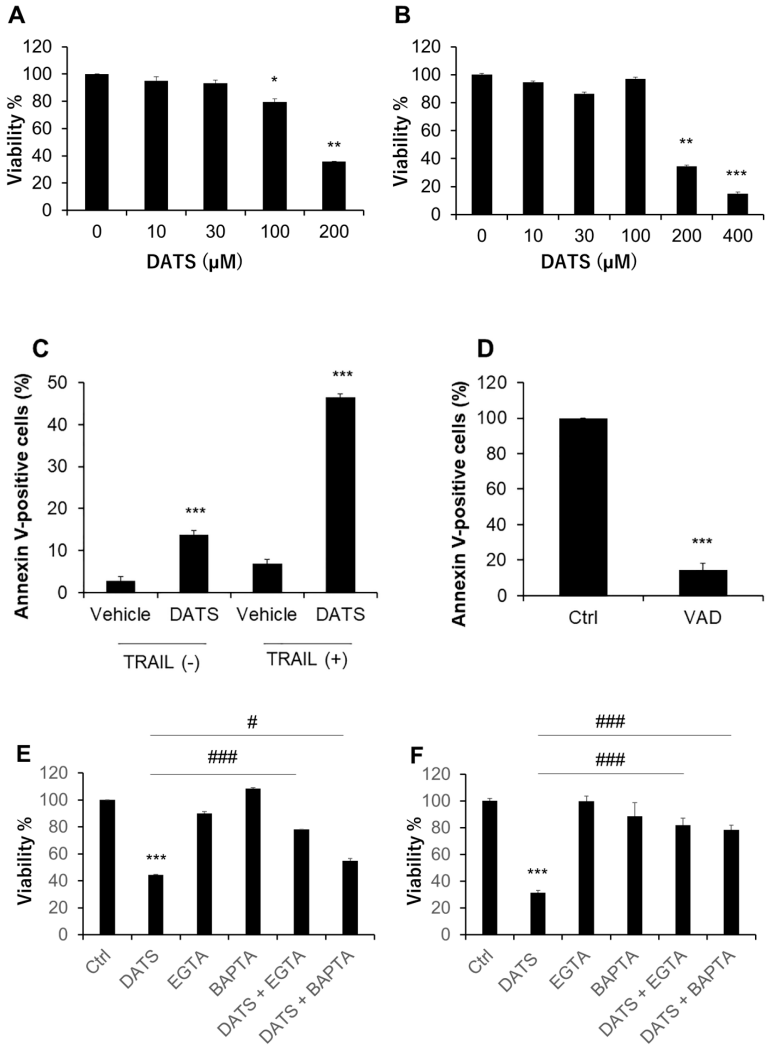

Figure 1. DATS exhibits the anti-melanoma effect in a caspase- and Ca^{2+}-dependent manner. (**A**) A375 and (**B**) A2058 cells in Dulbecco's modified Eagle's medium supplemented with 10% fetal calf serum (FCS/DMEM) were treated with the indicated concentrations of DATS for 72 h and analyzed for viability using the WST-8 assay. * $p < 0.05$; ** $p < 0.01$ vs. untreated control. (**C**) A375 cells were treated with DATS (100 μM) in the absence or presence of TRAIL (100 ng/mL) for 72 h, stained with FITC-conjugated annexin V and propidium iodide (PI), and analyzed in a flow cytometer. *** $p < 0.001$ vs. untreated control. (**D**) A375 cells were treated with DATS (200 μM) in the absence (Ctrl) or presence of Z-VAD-FMK (10 μM; VAD) for 72 h and processed as described above. *** $p < 0.001$ vs. DATS alone. (**E**,**F**) Effect of Ca^{2+} removal on the anti-melanoma effect. (**E**) A375 and (**F**) A2058 cells were treated with DATS (200 μM) in the absence or presence of EGTA (0.2 mM) or BAPTA (30 μM) for 72 h and analyzed for viability using the WST-8 assay. *** $p < 0.01$ vs. untreated control. # $p < 0.05$; ### $p < 0.001$ vs. DATS alone. Data represent the mean ± SD (n = 3–6).

2.2. Melittin Exhibits Anti-Melanoma Effect in a Ca^{2+}-Dependent Manner

Melittin is known to be a potent inducer of apoptosis in melanoma cells. Consistent with this view, treatment with the compound (≥2.5 μg/mL) for 72 h resulted in a robust increase in apoptotic (annexin V-positive) cells in A375 cells (Figure 2A). Meanwhile, the treatment minimally increased necrotic (annexin V-negative) cells. The extracellular Ca^{2+} removal by EGTA (0.5 mM) augmented the effect of the subtoxic dose (1 μg/mL) of melittin. On the other hand, it mitigated the increase in apoptosis while enhancing the increase in necrosis caused by the toxic concentration (5 μg/mL) of melittin (Figure 2B).

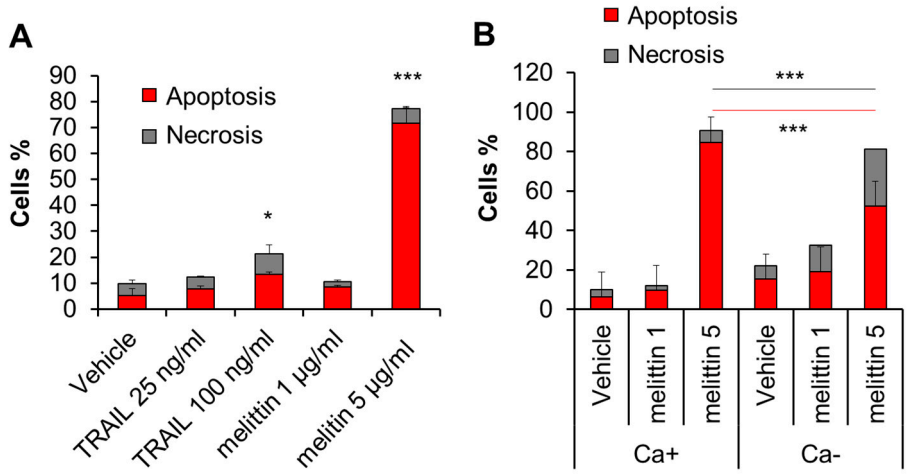

Figure 2. Melittin exhibits anti-melanoma effect in a Ca^{2+}-dependent manner. (**A**) A375 cells in FCS/DMEM were treated with the recombinant human TRAIL (25, 100 ng/mL) or melittin (1 or 5 μg/mL) alone for 72 h. (**B**) The cells were treated with melittin (1 or 5 μg/mL) in the absence (Ca+) or presence of EGTA (0.5 mM) (Ca−) for 72 h. The cells were evaluated for cell death modality as described in the legend of Figure 1. Data represent the mean ± SD (n = 3). * $p < 0.05$; *** $p < 0.001$.

2.3. DATS Increases $[Ca^{2+}]_{mit}$ without Increasing $[Ca^{2+}]_{cyt}$

Next, we determined whether DATS affected the intracellular Ca^{2+} level. First, we tested the effect on $[Ca^{2+}]_{cyt}$. We used the Ca^{2+}-ATPase inhibitor, thapsigargin (Tg), as a positive control, because it depletes the ER Ca^{2+} stores, thereby stimulating SOCE. Tg substantially increased $[Ca^{2+}]_{cyt}$, while DATS at the concentration of up to 200 μM minimally increased it (Figure 3A,B). On the other hand, DATS increased $[Ca^{2+}]_{mit}$ in a dose-dependent manner (Figure 3C,D). This increase occurred immediately, developed over time, and the effect of DATS (200 μM) was even higher than that induced by the positive control A23187 (5 μM).

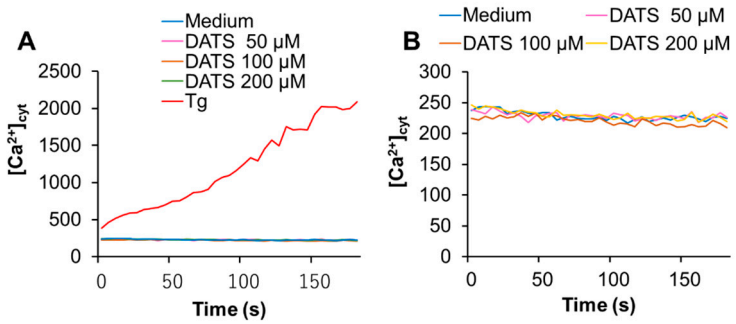

Figure 3. *Cont.*

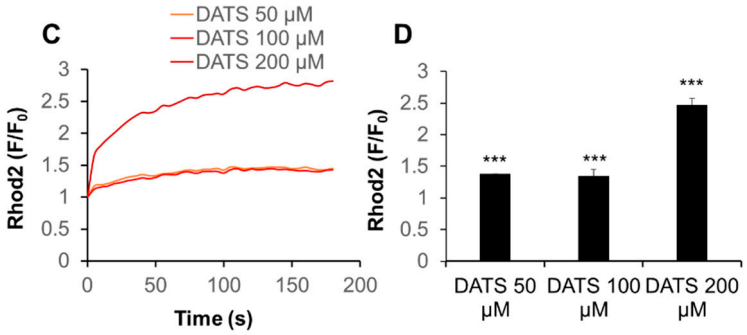

Figure 3. DATS induces $Ca^{2+}{}_{mit}$ overload with minimal $Ca^{2+}{}_{cyt}$ increase in melanoma cells. (**A**,**B**) DATS has minimal effect on $[Ca^{2+}]_{cyt}$. A375 cells were loaded with Fluo4-AM, added with DATS (50, 100, and 200 μM) or Tg (1 μM), and immediately measured for fluorescence for 3 min with excitation and emission at 485 and 538 nm, respectively, in a microplate fluorescence reader. $[Ca^{2+}]_{cyt}$ was evaluated as described in Materials and Methods. (**C**,**D**) DATS induces $Ca^{2+}{}_{mit}$ overload in a dose-dependent manner. The cells were loaded with dihydrorhod 2-AM, treated with DATS as described above, and measured for fluorescence with excitation and emission at 542 and 592 nm, respectively. Data are shown as F/F_0, where F and F_0 represent the fluorescence of the sample and control (medium-treated cells), respectively. Data shown in (**D**) represent the mean ± SE (n = 3). *** $p < 0.001$ vs. untreated control.

2.4. Melittin Increases Both $[Ca^{2+}]_{cyt}$ and $[Ca^{2+}]_{mit}$ in an Extracellular Ca^{2+}-Dependent Manner

The site-specific Ca^{2+} measurements showed that melittin (1.3–5 μg/mL) increased both $[Ca^{2+}]_{cyt}$ and $[Ca^{2+}]_{mit}$ in a dose-dependent manner (Figure 4A,C). Removal of the extracellular Ca^{2+} entirely abolished the increase in $[Ca^{2+}]_{cyt}$ but partially reduced the increase in $[Ca^{2+}]_{mit}$, indicating that these effects depend on the extracellular Ca^{2+} influx to different degrees (Figure 4B,D).

2.5. Acidification Has a Reciprocal Effect on $Ca^{2+}{}_{mit}$ Overload Caused by DATS and Melittin

The microenvironments, including the extracellular pH conditions, contribute to the various aspects of malignant phenotypes of cancer cells [27,28]. Therefore, we examined the effect of altered extracellular pH on $Ca^{2+}{}_{mit}$ overload. Cells were suspended in HBSS with different pH 6.8 and 7.4, treated with DATS, and measured for the intracellular Ca^{2+} levels. Notably, after DATS treatment, a small but significant increase in $[Ca^{2+}]_{cyt}$ was seen at pH 6.8, but not pH 7.4 (Figure 5A,B). Similarly, a greater extent of $Ca^{2+}{}_{mit}$ overload occurred at pH 6.8 compared to pH 7.4, and this impact was more pronounced for the higher concentration of the compound (Figure 5C,D). The effect was apparent for higher concentrations of DATS. Next, we analyzed the effect of the extracellular Ca^{2+} removal on $Ca^{2+}{}_{mit}$ overload seen under different pH. Cells were suspended in HBSS (pH 7.4 or 6.8) containing $CaCl_2$ or EGTA and treated with DATS. At pH 7.4, the Ca^{2+} removal almost entirely abolished the increase in $[Ca^{2+}]_{mit}$, while at pH 6.8, it reduced the increase only a modestly (Figure 5E,F). In contrast to DATS, acidification significantly mitigated $Ca^{2+}{}_{mit}$ overload caused by melittin. A much smaller increase in $[Ca^{2+}]_{mit}$ occurred at pH 6.8 compared to at pH 7.4 in response to a range of concentrations of melittin (1.3–5 μg/mL). Figure 5G shows the data for melittin (2.5 μg/mL). Notably, we observed a comparable level of $[Ca^{2+}]_{mit}$ increase in the cells placed in HBSS (pH 7.4) and Ca^{2+}-containing buffer. The $[Ca^{2+}]_{mit}$ rise seen in HBSS (pH 6.8) and Ca^{2+}-free buffer (pH 7.4) after melittin treatment were also comparable (Figure 5G,H).

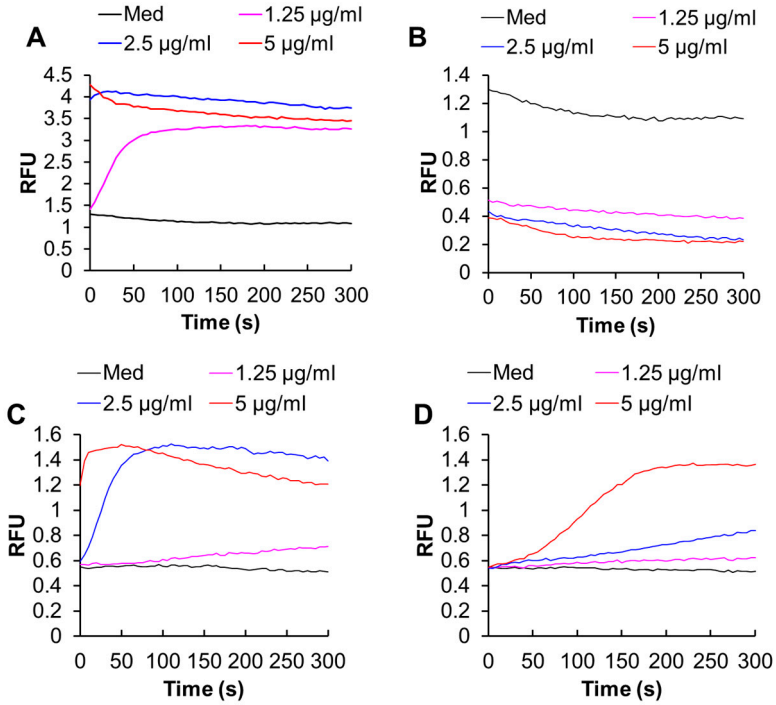

Figure 4. Melittin increases the intracellular Ca^{2+} levels in melanoma cells. (**A**,**B**) A375 cells were loaded with Fluo4-AM, suspended in HBSS containing 1 mM $CaCl_2$ (**A**) or 1 mM EGTA (**B**), and added with the indicated concentrations of melittin, and measured for fluorescence with excitation and emission at 485 and 538 nm, respectively in a microplate fluorescence reader. The vertical line shows relative fluorescence units (RFU). (**C**,**D**) The cells were loaded with dihydrorhod-2-AM, suspended in HBSS containing 1 mM $CaCl_2$ (**C**) or 1 mM EGTA (**D**), and added with the indicated concentrations of melittin, and measured for fluorescence with excitation and emission at 542 and 592 nm, respectively in a microplate fluorescence reader.

2.6. Acidification Mitigates SOCE

The data presented so far indicated that acidification reduced $Ca^{2+}{}_{mitt}$ overload caused by melittin. Since melittin is known as a potent activator of SOCE, we determined the effect of acidification on SOCE. We activated SOCE by the Ca^{2+} depletion-Ca^{2+} re-addition technique and examined the impact of acidification on the Ca^{2+} entry. At neutral extracellular pH, the addition of Tg to cells in a Ca^{2+}-free medium resulted in a small and transient increase in $[Ca^{2+}]_{cyt}$, indicating the Ca^{2+} release from the ER. The re-addition of Ca^{2+} to Tg-treated cells led to a higher and persistent increase in $[Ca^{2+}]_{cyt}$, and the inositol-1,4,5-triphosphate receptor (IP_3R)/SOCE antagonists 2-aminoethoxydiphenyl borate (2-APB) entirely blocked this Ca^{2+} response, verifying the onset of SOCE (Figure 6A). Even without any Ca^{2+} depletion in the ER (i.e., in the absence of Tg), a smaller but significant $[Ca^{2+}]_{cyt}$ rise was seen following Ca^{2+} re-addition and was minimally affected by 2-APB (Figure 6A, Right), indicating the onset of a store-independent Ca^{2+} influx (non-SOCE). Meanwhile, at pH 6.8, no substantial SOCE was observed, while the non-SOCE was increased by the acidification (Figure 6B).

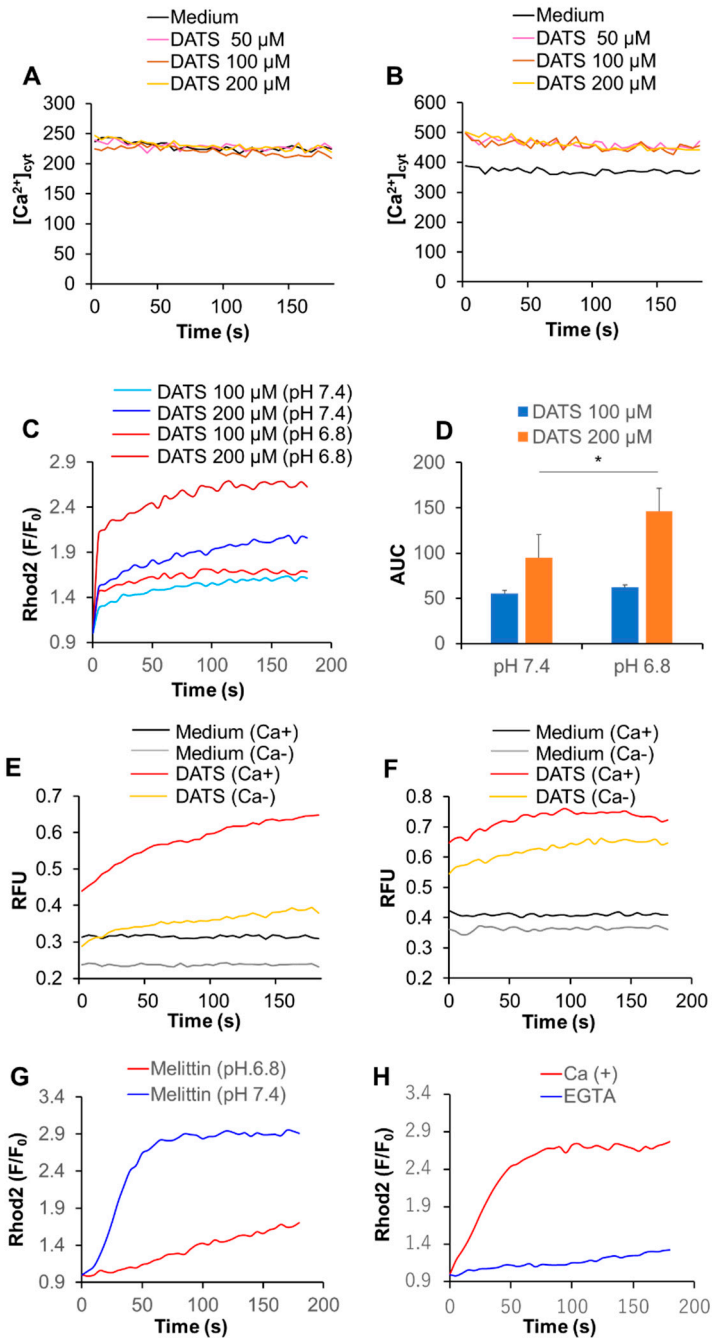

Figure 5. Acidification has a reciprocal effect on Ca^{2+}_{mit} overload caused by DATS and melittin. (**A**,**B**) A375 cells were suspended in HBSS (pH 7.4) (**A**) and 6.8 (**B**), treated with the indicated concentrations of DATS, and measured for fluorescence with excitation and emission at 485 and 538 nm, respectively in a microplate fluorescence reader. (**C**,**D**) Dihydrorhod2-AM-loaded A375 cells were suspended in HBSS (pH 7.4 or 6.8), treated with DATS (100 and 200 μM) and measured for fluorescence with excitation and emission at 542 and 592 nm, respectively, in a microplate fluorescence reader. Data are shown as F/F_0, where F and F_0 represent the fluorescence of the sample and control, respectively (n = 3–5). The data shown in (**D**) represent mean ± SD of the area under the curve (AUC) for 3 min (n = 3). (**E**,**F**) The cells were suspended in HBSS, pH 7.4 (**E**) or 6.8 (**F**) containing 1 mM $CaCl_2$ (Ca+) or 1 mM EGTA (Ca−), treated with DATS (200 μM), and measured for the fluorescence as described above. Data are shown as relative fluorescence unit (RFU). (**G**,**H**) The cells were suspended in HBSS (pH 7.4 or 6.8) (**G**) or HBSS (pH 7.4) containing 1 mM $CaCl_2$ (Ca+) or 1 mM EGTA (Ca−) (**H**), treated with melittin (2.5 μg/mL) and measured for the fluorescence. * $p < 0.05$.

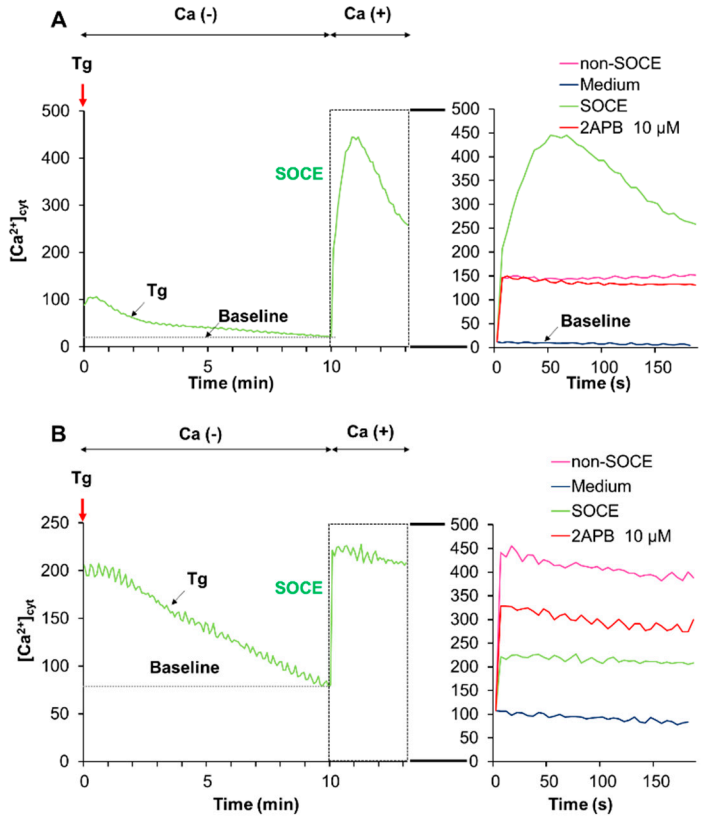

Figure 6. Acidification mitigates store-operated Ca^{2+} entry (SOCE). Fluo4-AM-loaded A375 cells were suspended in a Ca^{2+}-free HBSS supplemented with 1 mM EGTA at pH 7.4 (**A**) or pH 6.8 (**B**), added with thapsigargin (Tg, 2 μM, red arrow) and incubated for 10 min to deplete intracellular Ca^{2+} stores. Then, two mM Ca^{2+} was added to the cells (SOCE). After the addition of Tg, the fluorescence was monitored with excitation and emission at 485 and 538 nm, respectively. For validating SOCE, the cells in the Ca^{2+}-free buffer were treated as described above in the presence of 2-APB (10 μM). For non-SOCE measurement, the cells in the Ca^{2+}-free buffer were treated with the medium and then added with 2 mM Ca^{2+} (non-SOCE). Note that at pH 7.4, a higher increase in $[Ca^{2+}]_{cyt}$ was seen in the SOCE trace compared to the non-SOCE trace, and this effect was entirely abolished by 2-APB. Meanwhile, no such effect was seen at pH 6.8.

2.7. *Ca^{2+} Channel Blockers Inhibit $Ca^{2+}{}_{mit}$ Overload and Cell Death Caused by DATS*

To gain insight into the transport pathway(s) involved $Ca^{2+}{}_{mitt}$ overload caused by DATS, we look for Ca^{2+} channel antagonists affecting the $[Ca^{2+}]_{mit}$ rise. Eventually, we found that the Ca^{2+} channel blockers nifedipine, verapamil, and diltiazem significantly inhibited the effect of DATS. The inhibitory effect was seen more pronouncedly at pH 6.8 than at pH 7.4 (Figure 7A). Under the acidic conditions, nifedipine exhibited the most potent effect (70% reduction), while the other compounds inhibited it around 50% (Figure 7A). 2-APB had an inhibitory effect comparable to verapamil and diltiazem. Meanwhile, at the neutral pH conditions, these inhibitors mitigated the $[Ca^{2+}]_{mit}$ rise only modestly (20%; Figure 7A). Next, we examined the effect of Ca^{2+} blockers on the anti-melanoma effect in highly growing cells. Nifedipine, verapamil, and diltiazem significantly inhibited the anti-melanoma effect of DATS (200 μM; Figure 7B).

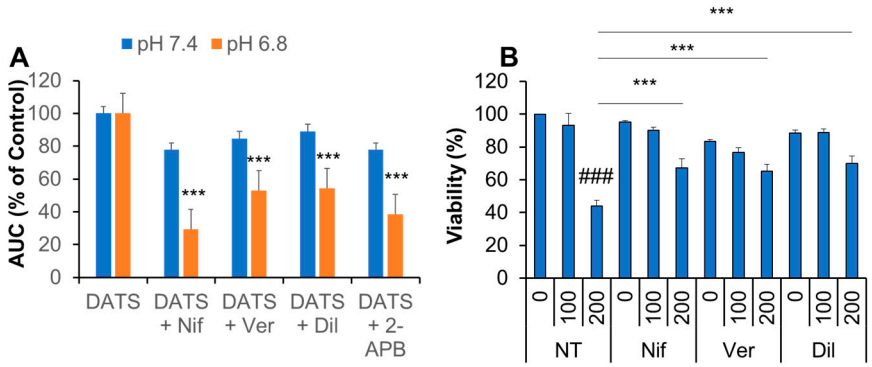

Figure 7. Ca^{2+} blockers inhibit $Ca^{2+}{}_{mit}$ overload and the anti-melanoma effect by DATS. (**A**) Dihydrorhod2-AM-loaded A375 cells suspended in HBSS, pH 6.8 were added with DATS (200 μM) in the absence or presence of 1 μM each of nifedipine (Nif), verapamil (Ver), diltiazem (Dil), or 2-APB (10 μM) and measured for fluorescence with excitation and emission at 542 and 592 nm, respectively. The data represent mean ± SD of the area under the curve (AUC) for 3 min. The values of DATS alone are set as 100%. *** $p < 0.001$ vs. DATS alone ($n = 3$) (**B**) The cells were treated with DATS (100 and 200 μM) in the absence or presence of each inhibitor as described above for 72 h and measured for cell viability by the WST-8 assay. Data represent the mean ± SD ($n = 3$). ### $p < 0.001$ vs. untreated control set as 100%. *** $p < 0.001$ vs. DATS alone.

3. Discussion

In this study, we elucidated the possible role of Ca^{2+} dysregulation in the anti-melanoma effect of DATS with a particular interest in the Ca^{2+} pathways involved. We found that DATS induced caspase-dependent apoptosis in melanoma cells, although relatively high concentrations of DATS are required (Figure 1). These results are consistent with previous studies, including our own, which demonstrate that DATS induces apoptosis in a variety of cancer cell types [8–11,14]. We noticed that cell confluency considerably affected the sensitivity to the compound. Cells growing near confluent tended to be more susceptible than those growing at low confluency. In agreement with the previous reports by others [23,24], melittin also primarily induced apoptosis in the cells (Figure 2A). Moreover, we found that extracellular Ca^{2+} entry was necessary for apoptosis caused by DATS and melittin (Figures 1E,F and 2B). The $Ca^{2+}{}_{mit}$ uptake is generally due to so-called reservoir function of the organelles: the mitochondria take up Ca^{2+} in response to increased $[Ca^{2+}]_{cyt}$ thereby preventing excessive $[Ca^{2+}]_{cyt}$ rise while they release Ca^{2+} in response to decreased $[Ca^{2+}]_{cyt}$ thereby counteracting excessive $[Ca^{2+}]_{cyt}$ depletion. Notably, we found that DATS and melittin had different impacts on $[Ca^{2+}]_{cyt}$ and $[Ca^{2+}]_{mit}$. DATS substantially increased $[Ca^{2+}]_{mit}$, but not $[Ca^{2+}]_{cyt}$ (Figure 3), suggesting that the $Ca^{2+}{}_{mit}$ overload is a result of the activation of a specific Ca^{2+} transport pathway rather than a simple $Ca^{2+}{}_{mit}$ uptake. Meanwhile, melittin markedly increased $[Ca^{2+}]_{cyt}$ and $[Ca^{2+}]_{mit}$ (Figure 4). However, extracellular Ca^{2+} removal entirely abolished the former, while attenuated the latter partially (Figure 4B,D). These results suggest that the $[Ca^{2+}]_{cyt}$ rise primarily results from extracellular Ca^{2+} entry while the $[Ca^{2+}]_{mit}$ increase is due to Ca^{2+} transport of both extracellular and intracellular Ca^{2+}. Dysregulation of $[Ca^{2+}]_{mit}$ is a master cause of cell death. A fine-tuned increase in $[Ca^{2+}]_{mit}$ supports energy metabolism, cell activation, and cell survival, while $Ca^{2+}{}_{mitt}$ overload can damage mitochondrial integrity, thereby inducing mitochondrial permeability transition pore (MPTP) opening and the resulting release of apoptogenic proteins [28–30]. Collectively, we conclude that different Ca^{2+} transport pathways participate in the $Ca^{2+}{}_{mitt}$ overload and apoptosis caused by DATS and melittin (Figure 8).

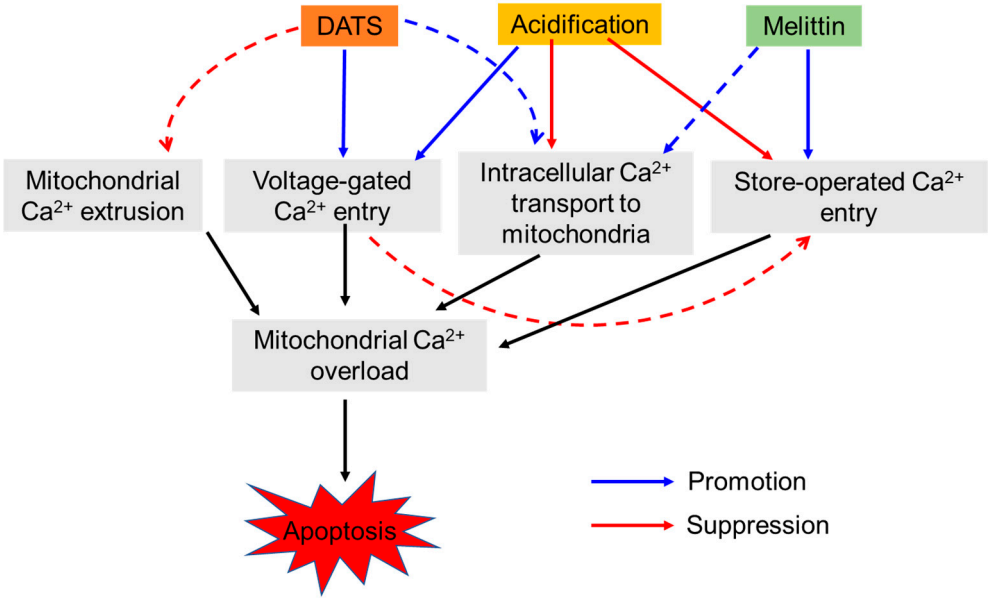

Figure 8. A schematic summary of the present study. Both DATS and melittin induce mitochondrial Ca^{2+} overload and apoptosis in melanoma cells. However, different pathways seem to contribute to the effects, depending on the apoptotic stimuli and the extracellular pH. Specifically, at neutral pH, the extracellular Ca^{2+} entry is predominant. Melittin primarily uses store-operated entry (SOCE), while DATS mainly utilizes yet unknown extracellular Ca^{2+} entry pathway possibly including voltage-gated Ca^{2+} entry (VGCE). Under acidic pH, SOCE is mitigated. In turn, intracellular Ca^{2+} entry plays a substantial role in the effects of melittin and DATS. Increased Ca^{2+} transport from the intracellular stores (e.g., the endoplasmic reticulum) to the mitochondria and decreased mitochondrial Ca^{2+} extrusion could contribute to the event. Under the acidic conditions, DATS, but not melittin, seems to utilize VGCE as the primary route for Ca^{2+} entry, leading to mitochondrial Ca^{2+} overload and apoptosis. The VGCE could exacerbate SOCE inactivation, and Ca^{2+} dysregulation due to the loss of the negative membrane potential, the driving force transporting extracellular Ca^{2+} into inner cells through SOCE.

Strikingly, DATS seems to evoke $Ca^{2+}{}_{mit}$ overload through different Ca^{2+} pathways, depending on the extracellular pH. At pH 7.4, DATS exhibits the effect mainly via the extracellular Ca^{2+} entry (Figure 5E), while at pH 6.8, DATS seemed to use both extracellular and intracellular Ca^{2} entry pathways (Figure 5F). Ca^{2+} released from the IP_3R can easily reach the mitochondrial matrix via the IP_3R–voltage-dependent anion channel (VDAC1)–mitochondrial Ca^{2+} uniporter (MCU) pathway [31,32]. The ER is the primary mechanism for regulating $[Ca^{2+}]_{mit}$ and tethered to mitochondria via a mitochondria-associated membrane; the physical association allows rapid Ca^{2+} transport through specified microdomains [33,34]. The IP_3R physically links to VDAC1 on the outer mitochondrial membrane and transports Ca^{2+} into the mitochondrial matrix [35,36]. We previously showed that $Ca^{2+}{}_{mit}$ remodeling in osteosarcoma cells was under the control of Ca^{2+} uptake through the MCU [37]. $[Ca^{2+}]_{mit}$ is also regulated by $Ca^{2+}{}_{mit}$ efflux through several different pathways, including the mitochondrial Na^{+}/Ca^{2+} exchanger (NCLX), Ca^{2+}/H^{+} antiporter, and MPTP [38–42]. Notably, our previous study showed that the NCLX inhibitor CGP-37157 causes $Ca^{2+}{}_{mit}$ overload and apoptosis in osteosarcoma cells [43]. Therefore, increased Ca^{2+} transport via the IP_3R–VDAC1–MCU pathway and decreased $Ca^{2+}{}_{mitt}$ extrusion could contribute to the $Ca^{2+}{}_{mitt}$ overload caused by DATS.

SOCE is the most ubiquitous pathway for Ca^{2+} transport from the extracellular space and activated following the depletion of Ca^{2+} stores from the ER. Recently, SOCE has emerged as critical machinery for Ca^{2+} influx, contributing to various malignant phenotypes in cancer cells [44–46]. SOCE is also shown to be responsible for cisplatin-induced apoptosis [20]. It is noteworthy that melittin can activate $iPLA_2$ to produce arachidonic acid and lysophospholipids and activates SOCE in vascular smooth muscle cells [25,26]. Given that melittin activates SOCE in melanoma cells, too, this action can expect

to cause massive Ca^{2+} dysregulation, as cisplatin does. A notable property of SOCE is its sensitivity to acidification; SOCE is suppressed by decreasing extracellular pH in several cell types [44,45]. In agreement with these reports, acidification entirely abolished SOCE in melanoma cells (Figure 6). Notably, the $Ca^{2+}{}_{mit}$ overload induced by melittin was mainly dependent upon extracellular Ca^{2+} entry and was suppressed by acidification (Figure 5). Extracellular Ca^{2+} removal and acidification caused a similar degree of reduction, suggesting that extracellular Ca^{2+} entry is specifically sensitive to acidification, as observed with SOCE. Together, our findings strongly suggest that melittin evokes $Ca^{2+}{}_{mit}$ overload via SOCE activation. This view is consistent with other reports demonstrating the requirement of SOCE for active $Ca^{2+}{}_{mit}$ uptake [47,48]. However, further studies, including the examination of the involvement of SOCE components such as STIM1 and ORAI1, are necessary for validation.

Another important finding in the present study is that Ca^{2+} channel blockers significantly mitigate $Ca^{2+}{}_{mit}$ overload and the anti-melanoma effect of DATS at acidic pH (Figure 7). These findings suggest a role of VGCE in $Ca^{2+}{}_{mit}$ overload and apoptosis. Notably, acidification increased $Ca^{2+}{}_{mit}$ overload caused by DATS (Figure 5), and sensitivity to Ca^{2+} channel blockers was higher at acidic pH than at neutral pH (Figure 7A). The latter finding seems to provide another evidence for the role of VGCE because Kato and colleagues have shown that an acidic pH (5.4–6.5) increases Ca^{2+} influx in mouse B16 melanoma cells through VGCE [49]. The activation of VGCE requires plasma membrane depolarization, which leads to the loss of the negative membrane potential, the driving force transporting extracellular Ca^{2+} into inner cells. Accordingly, SOCE could be compromised under these conditions. Thus, acidification activates VGCE while mitigates SOCE, thereby possibly playing a vital role in switching the Ca^{2+} entry pathway from SOCE to VGCE. The microenvironments of tumor cells are acidic due to an H^+ efflux caused by increased vacuolar ATPase activity, and this acidification causes multiple malignant phenotypes, including increased proliferation, drug resistance, and metastasis [27,28]. Therefore, our observations that high confluent cells are relatively high responders of DATS could be explained by the predominant role of VGCE under acidic extracellular microenvironments, because the extracellular pH drops in cells growing at high density.

There remain issues to be resolved in future studies. In particular, the identification of voltage-gated Ca^{2+} channels (VGCCs) involved in $Ca^{2+}{}_{mit}$ overload caused by DATS is challenging. Our preliminary experiments revealed that melanoma cells expressed $Ca_v1.2$ and $Ca_v1.3$ isoform of L-type VGCCs. Notably, the previous studies demonstrate the occurrence of the coordinate control of STIM1-ORAI1 and $Ca_v1.2$ [50,51]. Therefore, there is an intriguing possibility that $Ca_v1.2$ plays a role in $Ca^{2+}{}_{mit}$ overload via a specific interaction with SOCE. Further studies are necessary to clarify the molecular entity of VGCCs involved and to test this hypothesis.

In conclusion, the present study demonstrated that DATS and melittin exhibit the anti-melanoma effects by evoking pro-apoptotic $Ca^{2+}{}_{mit}$ overload through the different pathways, possibly VGCE and SOCE. Our findings suggest the involvement of multiple Ca^{2+} entry pathways in $Ca^{2+}{}_{mit}$ remodeling in melanoma cells and switching between them, depending on apoptotic stimuli and pH microenvironments.

4. Materials and Methods

4.1. Materials

All chemicals were purchased from Sigma Aldrich (St. Louis, MO, USA) unless otherwise specified. Alliin and allicin were obtained from Cayman Chemical Co. (Ann Arbor, MI, USA). Soluble recombinant human TRAIL was obtained from Enzo Life Sciences (San Diego, CA, USA). The pan-caspase inhibitor Z-VAD-FMK was purchased from Merck Millipore (Darmstadt, Germany). All insoluble reagents were dissolved in dimethylsulfoxide (DMSO) and diluted with high glucose-containing Dulbecco's modified Eagle's medium (DMEM) supplemented with 10% fetal bovine serum (FBS) or Hank's balanced salt

solution (HBSS; pH 7.4, Nissui Pharmaceutical Co., Ltd., Tokyo, Japan; final DMSO concentration, <0.1%) prior to use.

4.2. Cell Culture

Cells were cultured in 10% FBS/DMEM supplemented with 100 U/mL penicillin and 100 µg streptomycin (Pen-Strep, Thermo Fisher Scientific Japan, Tokyo, Japan) in a 95% air/5% CO_2 humidified atmosphere unless otherwise specified. The human melanoma cell lines A375 (cell number CRL-1619) and A2058 (cell number IFO 50276) were obtained from the American Type Culture Collection (ATCC, Manassas, VA, USA) and the Japanese Collection of Research Bioresources (JCRB) Cell Bank of National Institutes of Biomedical Innovation, Health, and Nutrition (Osaka, Japan), respectively. Cells were harvested by incubation with 0.25% trypsin-ethylenediaminetetraacetic acid (EGTA; Thermo Fisher Scientific, Waltham, MA, USA) for 5 min at 37 °C.

4.3. Cell Viability Assay

Cell viability was measured by WST-8 assay using Cell Counting Reagent SF (Nacalai Tesque, Inc., Kyoto, Japan) as previously described [43] with modifications. This method is a colorimetric assay based on the formation of a water-soluble formazan product. Briefly, cells were seeded at a density of 8×10^3 cells/well in 96-well plates (Corning Incorporated, Corning, NY, USA) and cultured with agents to be tested for 72 h at 37 °C before the addition of 10 µL of cell counting reagent SF and further incubation for 2 h. The absorbances were measured at 450 nm using an ARVO MX microplate reader (PerkinElmer Japan Co., Ltd., Yokohama, Japan).

4.4. Cell Death Assay

Cell death was quantitatively assessed by double-staining with fluorescein isothiocyanate (FITC)-conjugated annexin V and propidium iodide (PI) as previously described [37]. Briefly, cells plated in 24-well plates (2×10^5 cells/well) were treated with the agents to be tested for 20 h and stained with FITC-conjugated annexin V and PI using a commercially available kit (Annexin V FITC Apoptosis Detection Kit I: BD Biosciences, San Jose, CA, USA). The stained cells (10,000 cells) were analyzed in FL-1 and FL-2 channel of a FACSCalibur flow cytometer (BD Biosciences) using the CellQuest software (BD Biosciences). Four cellular subpopulations were evaluated: viable cells (annexin V-negative and PI-negative); early apoptotic cells (annexin V-positive and PI-negative); late apoptotic cells (annexin V-positive and PI-positive); and necrotic/membrane-damaged cells (annexin V-negative and PI-positive).

4.5. Intracellular Ca^{2+} Measurements

Changes in $Ca^{2+}{}_{cyt}$ and $Ca^{2+}{}_{mit}$ levels were measured using Fluo4-AM and rhod2-AM (Dojindo Kumamoto, Japan), respectively, as previously described [37]. For improvement of mitochondrial localization of rhod 2-AM [52], it was reduced to the colorless, nonfluorescent dihydrorhod 2-AM by sodium borohydride, according to the manufacturer's protocol. Cells were loaded with 4 µM each of Fluo 4-AM or dihydrorhod 2-AM for 40 min at 37 °C, washed with HBSS. Then, the cells (1×10^6/mL) were resuspended in HBSS in 96-well plates. The cells were manually added with the agents to be tested. Then, the cells were measured for fluorescence in a microplate reader (Fluoroskan Ascent, ThermoFisher Scientific) with excitation and emission at 485 and 538 nm (for Fluo 4-AM), respectively, and 542 and 592 nm (for rhod 2-AM), respectively. For the analysis of Ca^{2+} release and SOCE, Fluo4-AM-loaded cells were suspended in a Ca^{2+}-free medium (HBSS supplemented with 1 mM EGTA) and treated with 2 µM Tg for 10 min and then added to 2 mM $CaCl_2$. For analysis of non-SOCE, cells in the Ca^{2+}-free medium were treated with the medium for 10 min and then added to 2 mM $CaCl_2$.

4.6. Statistical Analysis

Data are presented as mean ± standard deviation (SD) or standard error (SE) and were analyzed by one-way analysis of variance followed by Tukey's post hoc test using add-in software for Excel 2016 for Windows (SSRI, Tokyo, Japan). $p < 0.05$ was considered statistically significant.

Author Contributions: Conceptualization, Y.S.-K.; methodology, T.O. and Y.S.-K.; validation, C.N., M.S.-K. (Manami Suzuki-Karasaki) and Y.S.-K.; investigation, C.N., M.S.-K. (Manami Suzuki-Karasaki), M.S.-K. (Miki Suzuki-Karasaki) and Y.S.-K.; resources, T.O.; data curation, C.N.; writing—original draft preparation, C.N., M.S.-K. (Manami Suzuki-Karasaki) and Y.S.-K.; writing—review and editing, T.O. and Y.S.-K.; supervision, T.O. and Y.S.-K.; project administration, T.O. and Y.S.-K.; funding acquisition, T.O. and Y.S.-K. All authors have read and agreed to the published version of the manuscript.

Funding: This research was funded by JSPS KAKENHI, grant number 15K09792, and 18K09121.

Acknowledgments: We thank the JCRB Cell Bank of National Institutes of Biomedical Innovation, Health, and Nutrition (Osaka, Japan) and the Riken BioResource Center (Tsukuba, Japan) for providing cell lines.

Conflicts of Interest: M.S.-K. (Manami Suzuki-Karasaki), M.S.-K. (Miki Suzuki-Karasaki), and Y.S.-K. are employees of the non-profit Institute Plasma ChemiBio Laboratory. Other authors have no conflicts of interest. The funders had no role in the design of the study; in the collection, analyses, or interpretation of data; in the writing of the manuscript, or in the decision to publish the results.

References

1. Tapiero, H.; Townsend, D.M.; Tew, K.D. Organosulfur compounds from alliaceae in the prevention of human pathologies. *Biomed. Pharmacother.* **2004**, *58*, 183–193. [CrossRef]
2. Kodera, Y.; Suzuki, A.; Imada, O.; Kasuga, S.; Sumioka, I.; Kanezawa, A.; Taru, N.; Fujikawa, M.; Nagae, S.; Masamoto, K.; et al. Physical, chemical, and biological properties of s-allylcysteine, an amino acid derived from garlic. *J. Agric. Food Chem.* **2002**, *50*, 622–632. [CrossRef]
3. Schäfer, G.; Kaschula, C.H. The immunomodulation and anti-inflammatory effects of garlic organosulfur compounds in cancer chemoprevention. *Anticancer Agents Med. Chem.* **2014**, *14*, 233–240. [CrossRef]
4. Sun, S.Y.; Hail, N., Jr.; Lotan, R. Apoptosis as a novel target for cancer chemoprevention. *J. Natl. Cancer Inst.* **2002**, *96*, 662–672. [CrossRef]
5. Hail, N., Jr.; Lotan, R. Cancer chemoprevention and mitochondria: Targeting apoptosis in transformed cells via the disruption of mitochondrial bioenergetics/redox state. *Mol. Nutr. Food Res.* **2009**, *53*, 49–67. [CrossRef]
6. Belman, S. Onion and garlic oils inhibit tumor promotion. *Carcinogenesis* **1983**, *4*, 1063–1065. [CrossRef] [PubMed]
7. Wang, H.C.; Pao, J.; Lin, S.; Sheen, L.Y. Molecular mechanisms of garlic-derived allyl sulfides in the inhibition of skin cancer progression. *Ann. N. Y. Acad. Sci.* **2012**, *1271*, 44–52. [CrossRef] [PubMed]
8. Das, A.; Banik, N.L.; Ray, S.K. Garlic compounds generate reactive oxygen species leading to activation of stress kinases and cysteine proteases for apoptosis in human glioblastoma T98G and U87MG cells. *Cancer* **2007**, *110*, 1083–1095. [CrossRef] [PubMed]
9. Karmakar, S.; Banik, N.L.; Patel, S.J.; Ray, S.K. Garlic compounds induced calpain and intrinsic caspase cascade for apoptosis in human malignant neuroblastoma SH-SY5Y cells. *Apoptosis* **2007**, *12*, 671–684. [CrossRef] [PubMed]
10. Powolny, A.A.; Singh, S.V. Multitargeted prevention and therapy of cancer by diallyl trisulfide and related Allium vegetable-derived organosulfur compounds. *Cancer Lett.* **2008**, *269*, 305–314. [CrossRef]
11. Busch, C.; Jacob, C.; Anwar, A.; Burkholz, T.; Aicha Ba, L.; Cerella, C.; Diederich, M.; Brandt, W.; Wessjohann, L.; Montenarh, M. Diallylpolysulfides induce growth arrest and apoptosis. *Int. J. Oncol.* **2010**, *36*, 743–749. [PubMed]
12. Shankar, S.; Chen, Q.; Ganapathy, S.; Singh, K.P.; Srivastava, R.K. Diallyl trisulfide increases the effectiveness of TRAIL and inhibits prostate cancer growth in an orthotopic model: Molecular mechanisms. *Mol. Cancer Ther.* **2008**, *7*, 2328–2338. [CrossRef] [PubMed]
13. Suzuki-Karasaki, Y.; Suzuki-Karasaki, M.; Uchida, M.; Ochiai, T. Depolarization Controls TRAIL-Sensitization and Tumor-Selective Killing of Cancer Cells: Crosstalk with ROS. *Front. Oncol.* **2014**, *4*, 128. [CrossRef] [PubMed]

14. Murai, M.; Inoue, T.; Suzuki-Karasaki, M.; Ochiai, T.; Ra, C.; Nishida, S.; Suzuki-Karasaki, Y. Diallyl trisulfide sensitizes human melanoma cells to TRAIL-induced cell death by promoting endoplasmic reticulum-mediated apoptosis. *Int. J. Oncol.* **2012**, *41*, 2029–2037. [CrossRef]
15. Dyer, M.J.; MacFarlane, M.; Cohen, G.M. Barriers to effective TRAIL-targeted therapy of malignancy. *J. Clin. Oncol.* **2007**, *25*, 4505–4506. [CrossRef]
16. Dimberg, L.Y.; Anderson, C.K.; Camidge, R.; Behbakht, K.; Thorburn, A.; Ford, H.L. On the TRAIL to successful cancer therapy? Predicting and counteracting resistance against TRAIL-based therapeutics. *Oncogene* **2013**, *32*, 1341–1350. [CrossRef]
17. Mellier, G.; Pervaiz, S. The three Rs along the TRAIL: Resistance, re-sensitization and reactive oxygen species (ROS). *Free Radic. Res.* **2012**, *46*, 996–1003. [CrossRef]
18. Inoue, T.; Suzuki-Karasaki, Y. Mitochondrial superoxide mediates mitochondrial and endoplasmic reticulum dysfunctions in TRAIL-induced apoptosis in Jurkat cells. *Free Radic. Biol. Med.* **2013**, *61*, 273–284. [CrossRef]
19. Suzuki-Karasaki, M.; Ochiai, T.; Suzuki-Karasaki, Y. Crosstalk between mitochondrial ROS and depolarization in the potentiation of TRAIL-induced apoptosis in human tumor cells. *Int. J. Oncol.* **2014**, *44*, 616–628. [CrossRef]
20. Gualdani, R.; de Clippele, M.; Ratbi, I.; Gailly, P.; Tajeddine, N. Store-Operated Calcium Entry Contributes to Cisplatin-Induced Cell Death in Non-Small Cell Lung Carcinoma. *Cancers* **2019**, *11*, 430. [CrossRef]
21. Zhao, M.; Brunk, U.T.; Eaton, J.W. Delayed oxidant-induced cell death involves activation of phospholipase A2. *FEBS Lett.* **2001**, *509*, 399–404. [CrossRef]
22. Oršolić, N. Bee venom in cancer therapy. *Cancer Metastasis Rev.* **2012**, *31*, 173–194. [CrossRef] [PubMed]
23. Chu, S.T.; Cheng, H.H.; Huang, C.J.; Chang, H.C.; Chi, C.C.; Su, H.H.; Hsu, S.S.; Wang, J.L.; Chen, I.S.; Liu, S.I.; et al. Phospholipase A2-independent Ca^{2+} entry and subsequent apoptosis induced by melittin in human MG63 osteosarcoma cells. *Life Sci.* **2007**, *80*, 364–369. [CrossRef] [PubMed]
24. Sharma, S.V. Melittin-induced hyperactivation of phospholipase A2 activity and calcium influx in ras-transformed cells. *Oncogene* **1993**, *8*, 939–947. [PubMed]
25. Smani, T.; Zakharov, S.I.; Leno, E.; Csutora, P.; Trepakova, E.S.; Bolotina, V.M. Ca^{2+}-independent phospholipase A2 is a novel determinant of store-operated Ca^{2+} entry. *J. Biol. Chem.* **2003**, *278*, 11909–11915. [CrossRef] [PubMed]
26. Smani, T.; Zakharov, S.I.; Csutora, P.; Leno, E.; Trepakova, E.S.; Bolotina, V.M. A novel mechanism for the store-operated calcium influx pathway. *Nat. Cell Biol.* **2004**, *6*, 113–120. [CrossRef] [PubMed]
27. Whitton, B.; Okamoto, H.; Packham, G.; Crabb, S.J. Vacuolar ATPase as a potential therapeutic target and mediator of treatment resistance in cancer. *Cancer Med.* **2018**, *7*, 3800–3811. [CrossRef]
28. Pamarthy, S.; Kulshrestha, A.; Katara, G.K.; Beaman, K.D. The curious case of vacuolar ATPase: Regulation of signaling pathways. *Mol. Cancer* **2018**, *17*, 41. [CrossRef]
29. Nicotera, P.; Zhivotovsky, B.; Orrenius, S. Nuclear calcium transport and the role of calcium in apoptosis. *Cell Calcium* **1994**, *16*, 279–288. [CrossRef]
30. Green, D.R.; Reed, J.C. Mitochondria and apoptosis. *Science* **1998**, *281*, 1309–1312. [CrossRef]
31. Zhu, L.P.; Yu, X.D.; Ling, S.; Brown, R.A.; Kuo, T.H. Mitochondrial Ca^{2+} homeostasis in the regulation of apoptotic and necrotic cell deaths. *Cell Calcium* **2000**, *28*, 107–117. [CrossRef] [PubMed]
32. Kania, E.; Roest, G.; Vervliet, T.; Parys, J.B.; Bultynck, G. IP_3 Receptor-Mediated Calcium Signaling and Its Role in Autophagy in Cancer. *Front. Oncol.* **2017**, *7*, 140. [CrossRef] [PubMed]
33. Pedriali, G.; Rimessi, A.; Sbano, L.; Giorgi, C.; Wieckowski, M.R.; Previati, M.; Pinton, P. Regulation of Endoplasmic Reticulum-Mitochondria Ca^{2+} Transfer and Its Importance for Anti-Cancer Therapies. *Front. Oncol.* **2017**, *7*, 180. [CrossRef]
34. Rizzuto, R.; Pozzan, T. Microdomains of intracellular Ca^{2+}: Molecular determinants and functional consequences. *Physiol. Rev.* **2006**, *86*, 369–408. [CrossRef] [PubMed]
35. Giacomello, M.; Pellegrini, L. The coming of age of the mitochondria-ER contact: A matter of thickness. *Cell Death Differ.* **2016**, *23*, 1417–1427. [CrossRef] [PubMed]
36. Marchi, S.; Pinton, P. The mitochondrial calcium uniporter complex: Molecular components, structure and physiopathological implications. *J. Physiol.* **2014**, *592*, 829–839. [CrossRef] [PubMed]
37. Takata, N.; Ohshima, Y.; Suzuki-Karasaki, M.; Yoshida, Y.; Tokuhashi, Y.; Suzuki-Karasaki, Y. Mitochondrial Ca^{2+} removal amplifies TRAIL cytotoxicity toward apoptosis-resistant tumor cells via promotion of multiple cell death modalities. *Int. J. Oncol.* **2017**, *51*, 193–203. [CrossRef]

38. Brand, M.D. Electroneutral efflux of Ca^{2+} from liver mitochondria. *Biochem. J.* **1985**, *225*, 413–419. [CrossRef]
39. Altschuld, R.A.; Hohl, C.M.; Castillo, L.C.; Garleb, A.A.; Starling, R.C.; Brierley, G.P. Cyclosporin inhibits mitochondrial calcium efflux in isolated adult rat ventricular cardiomyocytes. *Am. J. Physiol.* **1992**, *262*, 1699–1704.
40. Bernardi, P.; von Stockum, S. The permeability transition pore as a Ca^{2+} release channel: New answers to an old question. *Cell Calcium* **2012**, *52*, 22–27. [CrossRef]
41. Di Lisa, F.; Carpi, A.; Giorgio, V.; Bernardi, P. The mitochondrial permeability transition pore and cyclophilin D in cardioprotection. *Biochim. Biophys. Acta* **2011**, *1813*, 1316–1322. [CrossRef] [PubMed]
42. Gutiérrez-Aguilar, M.; Baines, C.P. Structural mechanisms of cyclophilin D-dependent control of the mitochondrial permeability transition pore. *Biochim. Biophys. Acta* **2014**, *1850*, 2041–2047. [CrossRef] [PubMed]
43. Ohshima, Y.; Takata, N.; Suzuki-Karasaki, M.; Yoshida, Y.; Tokuhashi, Y.; Suzuki-Karasaki, Y. Disrupting mitochondrial Ca^{2+} homeostasis causes tumor-selective TRAIL sensitization through mitochondrial network abnormalities. *Int. J. Oncol.* **2017**, *51*, 1146–1158. [CrossRef] [PubMed]
44. Bergmeier, W.; Weidinger, C.; Zee, I.; Feske, S. Emerging roles of store-operated Ca^{2+} entry through STIM and ORAI proteins in immunity, hemostasis, and cancer. *Channels* **2013**, *7*, 379–391. [CrossRef]
45. Jardin, I.; Rosado, J.A. STIM and calcium channel complexes in cancer. *Biochim. Biophys. Acta* **2016**, *1863*, 1418–1426. [CrossRef]
46. Chalmers, S.B.; Monteith, G.R. ORAI channels and cancer. *Cell Calcium* **2018**, *74*, 160–167. [CrossRef]
47. Deak, A.T.; Blass, S.; Khan, M.J.; Groschner, L.N.; Waldeck-Weiermair, M.; Hallström, S.; Graier, W.F.; Malli, R. RIP3-mediated STIM1 oligomerization requires intact mitochondrial Ca^{2+} uptake. *J. Cell Sci.* **2014**, *127*, 2944–2955. [CrossRef]
48. Elustondo, P.A.; Nichols, M.; Robertson, G.S.; Pavlov, E.V. Mitochondrial Ca^{2+} uptake pathways. *J. Bioenerg. Biomembr.* **2017**, *49*, 113–119. [CrossRef]
49. Kato, Y.; Ozawa, S.; Tsukuda, M.; Kubota, E.; Miyazaki, K.; St-Pierre, Y.; Hata, R. Acidic extracellular pH increases calcium influx-triggered phospholipase D activity along with acidic sphingomyelinase activation to induce matrix metalloproteinase-9 expression in mouse metastatic melanoma. *FEBS. J.* **2007**, *274*, 3171–3183. [CrossRef]
50. Wang, Y.; Deng, X.; Mancarella, S.; Hendron, E.; Eguchi, S.; Soboloff, J.; Tang, X.D.; Gill, D.L. The calcium store sensor, STIM1, reciprocally controls Orai and CaV1.2 channels. *Science* **2010**, *330*, 105–109. [CrossRef]
51. Dionisio, N.; Smani, T.; Woodard, G.E.; Castellano, A.; Salido, G.M.; Rosado, J.A. Homer proteins mediate the interaction between STIM1 and Cav1.2 channels. *Biochim. Biophys. Acta* **2015**, *1853*, 1145–1153. [CrossRef] [PubMed]
52. Hajnóczky, G.; Robb-Gaspers, L.D.; Seitz, M.B.; Thomas, A.P. Decoding of cytosolic calcium oscillations in the mitochondria. *Cell* **1995**, *82*, 415–424. [CrossRef]